# Estimating Blade Section Airloads from Blade Leading–Edge Pressure Measurements

JOHANNES M. VAN AKEN

*AerospaceComputing, Inc.*
*Army/NASA Rotorcraft Division*
*NASA Ames Research Center*
*Moffett Field, California*

The Tilt-Rotor Aeroacoustic Model (TRAM) test in the Duitse-Nederlandse Wind (DNW) Tunnel acquired blade pressure data for forward flight test conditions of a tiltrotor in helicopter mode. Chordwise pressure data at seven radial locations were integrated to obtain the blade section normal force. The present investigation evaluates the use of linear regression analysis and of neural networks in estimating the blade section normal force coefficient from a limited number of blade leading-edge pressure measurements and representative operating conditions. These network models are subsequently used to estimate the airloads at intermediate radial locations where only blade pressure measurements at the 3.5% chordwise stations are available.

## Nomenclature

| | |
|---|---|
| a | speed of sound |
| A | rotor disk area, $\pi R^2$ |
| c | local blade chord |
| $c_{ref}$ | blade reference chord |
| $c_n$ | blade section normal force coefficient, $N/(^1/_2\rho U^2 c)$ |
| $c_p$ | pressure coefficient, $p/(^1/_2\rho U^2)$ |
| $C_T$ | rotor thrust coefficient, $T/\rho(\Omega R)^2 A$ (shaft axes) |
| M | Mach number |
| $M_{tip}$ | blade tip Mach number, $\Omega R/a$ |
| nn | neural network |
| p | local blade pressure |
| r | blade radial station (0 to R) |
| R | blade radius |
| U | local velocity |
| V | free stream velocity; wind tunnel speed |
| $\alpha$, $a_{shaft}$ | rotor shaft angle (positive aft) |
| $\mu$, mu | advance ratio, $V/\Omega R$ |
| $\rho$ | air density |
| $\sigma$ | rotor solidity, $Nc_{ref}/(\pi R)$ ($\sigma$ = 0.105 for TRAM) |
| $\psi$, az | blade azimuth angle (zero azimuth is downstream) |
| $\Omega$ | rotor rotational speed |

## Introduction

The tiltrotor aircraft configuration has the potential of revolutionizing the air transportation system by providing an economical combination of vertical take-off and landing capability with efficient high-speed cruise flight. To achieve this potential NASA has invested heavily in tilt rotor research, both experimentally (Refs. 1-2) and theoretically (Refs. 3-4).

During recent wind tunnel testing of the Tilt-Rotor Aeroacoustic Model (TRAM), blade pressure measurements were acquired from some 150 pressure transducers, distributed over two of the three TRAM rotor blades. These blade pressures allowed for the computation of the blade section normal force coefficient at several radial stations.

The present investigation evaluates the use of linear regression and of neural networks in estimating blade section airloads from blade leading edge pressures and

*Presented at the American Helicopter Society 59th Annual Forum, Phoenix, Arizona, May 6-8, 2003.* 

representative test conditions. The objective of the present study is three-fold: a) evaluate the ability of regression and neural network models to estimate blade section airloads from leading edge pressure data; b) evaluate the ability of such models to estimate the airloads at a radial location where bad pressure transducer(s) prevented the computation of $c_n$ from detailed chordwise pressure data; and c) evaluate these models in estimating the airloads at those radial stations where only pressure data at the 3.5% chord-wise station were available.

## Previous Work

Other researchers (Refs. 5-8) have reported on using leading edge pressure measurements to estimate blade section airloads.

References 5-7 describe a technique used at Royal Aerospace Establishment (RAE) of using a pressure sensor near the leading edge of the rotor blade to determine the incidence, $\alpha$, and local aerodynamic loading, $c_n$, using a comprehensive look-up table compiled from two-dimensional airfoil characteristics with suitable allowance made for the various unsteady effects. The pressure instrumented blade described in Ref. 6 had an array of 20 leading edge and 20 trailing edge pressure sensors. The leading edge sensors are located at 2% chord in the upper blade surface and their position was chosen to minimize structural weakening of the blade resulting from the small depression in the blade spar necessary to accommodate the transducer into the profile. Reference 5 states that leading edge locations in the range from 0 to 3% chord would in general be suitable for use in the described technique. The trailing edge sensors are used to indicate the presence of stall (Ref. 5). The "stall indicator" sensors were externally mounted at 98% chord and were locally blended into the surface by a fairing, which should had minimal effect on the flow in this region.

Reference 8 discusses the deduction of the local airload, $c_n$, from the pressure data obtained from a few stations near the leading edge for the Higher-Harmonics Control Aeroacoustic Rotor Test (HART). One blade of the BO-105 model rotor was equipped with 124 pressure sensors. Three radial sections (0.75R, 0.87R, and 0.97R) were fully instrumented with 24 or 44 sensors. Sensors were located in the upper and lower blade surface at the 3% chord location at six radial locations (0.6R, 0.7R, 0.8R, 0.9R, 0.94R and 0.99R). Data from the fully instrumented sections were used to correlate the section airloads, $c_n$, to the $c_p$-data at the 3% chord location assuming a linear transfer function of the form $c_n=a*X+b$. Reference 8 looked at using only upper surface pressure, $X=c_{p,upper}$, using the difference between upper and lower pressure, $X=\Delta c_p$, and using upper and lower pressures as separate inputs to the transfer function (i.e., $c_n=a_1*c_{p,upper}+a_2*c_{p,lower}+b$). The pressure difference at 3% chord at the 0.62R location were used to estimate the local airloads using the transfer function obtained from the data for the 0.75R station. Reference 8 states that it would be preferable to use the data from a more downstream station than at 3% chord. In fact, it uses the transfer function determined from 9% chord data at the fully instrumented sections for the airloads computation from pressure data in a noise prediction code, called CONGA (Computation of Noise using Gauges Aerodynamics).

## TRAM Physical Description

The TRAM was designed as a 1/4-scale V-22 tiltrotor aircraft model. The rotor has a diameter of 9.5 ft. Details of the TRAM physical description can be found in Ref. 1.

The rotor blades and hub are designed as geometrically and dynamically scaled models of the V-22 blades. The hub is gimbaled with a constant velocity joint consisting of a spherical bearing and elastomeric torque links. The balance and flex-coupling measure forces and torque. The blade set has both strain-gauged and pressure-instrumented blades. There are 150 pressure transducers distributed over two blades: primarily at radial stations 0.50, 0.62, 0.82, and 0.96 on blade #1, and at radial stations 0.33, 0.72, 0.90, and 0.98 on blade #2 (see Table 1). At seven intermediate radial locations (r/R=0.93, 0.87, 0.77, 0.67, 0.56, and 0.42) pressure measurements were acquired only at the 3.5% chord-wise station. The pressure measurements can be integrated chordwise to obtain blade section normal force at seven primary radial stations (insufficient chordwise points are available at the 0.98 station). Reference 2 describes the data reduction process for the blade pressures and section normal force. The third blade carries all of the required safety of flight strain gauge instrumentation.

Because of instrumentation problems not all pressure transducers were functional at all times. At the start of the test, 135 of the pressure gauges were operational (see Table 1). For some test conditions, bad pressure transducer signals resulted in the inability to compute the blade section normal force coefficient at all seven radial stations.

**Table 1 Blade pressure instrumentation**

| | Chordwise position of pressure measurements, % chord, on upper (U) and lower (L) blade surface | | | | | | | | | | | | | | | | | | | | | | | |
|---|---|---|---|---|---|---|---|---|---|---|---|---|---|---|---|---|---|---|---|---|---|---|---|---|
| | 2.0 | | 3.5 | | 6.5 | | 10.5 | | 15.0 | | 21.0 | | 30.0 | | 37.5 | | 45.0 | | 52.5 | | 65.0 | | 90.0 | |
| r/R | U | L | U | L | U | L | U | L | U | L | U | L | U | L | U | L | U | L | U | L | U | L | U | L |
| 0.98 | | | 2 | 2 | | | 2 | 2 | | | | | 2 | 2 | | | | | | | 2 | 2 | | |
| 0.96 | ***1*** | 1 | ***1*** | 1 | ***1*** | 1 | 1 | 1 | 1 | 1 | 1 | 1 | 1 | 1 | 1 | | 1 | 1 | 1 | | 1 | 1 | 1 | 1 |
| | | | 2 | 2 | | | | | | | | | | | | | | | | | | | | |
| 0.93 | | | 2 | 2 | | | | | | | | | | | | | | | | | | | | |
| 0.90 | 2 | 2 | 2 | 2 | 2 | 2 | 2 | 2 | 2 | | 2 | 2 | 2 | | | | 2 | 2 | | | 2 | 2 | 2 | 2 |
| | | | 1 | 1 | | | | | | | | | | | | | | | | | | | | |
| 0.87 | | | 2 | 2 | | | | | | | | | | | | | | | | | | | | |
| 0.82 | 1 | ***1*** | 1 | ***1*** | 1 | ***1*** | 1 | 1 | 1 | | 1 | 1 | 1 | | | | 1 | 1 | | | 1 | 1 | 1 | 1 |
| | | | 2 | 2 | | | | | | | | | | | | | | | | | | | | |
| 0.77 | | | 2 | 2 | | | | | | | | | | | | | | | | | | | | |
| 0.72 | 2 | ***2*** | 2 | 2 | ***2*** | ***2*** | 2 | 2 | 2 | | 2 | 2 | 2 | | | | 2 | 2 | | | 2 | 2 | 2 | 2 |
| 0.67 | | | ***2*** | 2 | | | | | | | | | | | | | | | | | | | | |
| 0.62 | 1 | ***1*** | 1 | 1 | 1 | 1 | 1 | 1 | | | 1 | 1 | | | | | 1 | 1 | | | 1 | 1 | 1 | 1 |
| 0.56 | | | 2 | ***2*** | | | | | | | | | | | | | | | | | | | | |
| 0.50 | 1 | 1 | 1 | 1 | 1 | 1 | 1 | 1 | | | 1 | 1 | | | | | 1 | 1 | | | 1 | 1 | 1 | 1 |
| 0.42 | | | 2 | 2 | | | | | | | | | | | | | | | | | | | | |
| 0.33 | ***2*** | 2 | 2 | ***2*** | ***2*** | 2 | 2 | 2 | | | 2 | 2 | | | | | 2 | 2 | | | 2 | 2 | 2 | 2 |

Numbers 1 and 2 indicate that the pressure transducer is on blade 1 or blade 2, respectively.

Shaded numbers 1 and 2 indicate that the pressure transducer is non-operational at start of test.

Red/bold/italic numbers ***1 and 2*** indicate that the pressure transducer is non-operational for some of the considered twelve test points (identification for 2.0%, 3.5%, and 6.5% chordwise stations only).

## Data Reduction

The pressure measurements were sampled at 2048 per-rev. and data were collected for 64 revolutions. The pressure data in this report are a single revolution of data obtained by averaging over the 64 revolutions collected. To eliminate high frequency noise, a fast Fourier transform (FFT) is performed on the single revolution of airloads data and only the first 64 harmonics are maintained; an inverse FFT is performed to reconstruct the time history of 128 points in a revolution (reduced from 1024 harmonics representing 2048 samples). All the blade-vortex interaction events in the section normal force data are captured using 64 harmonics.

The measured balance loads of the TRAM in the DNW are corrected for model weight tares, aerodynamic tares, and for the influence of the wind tunnel walls. Details can be found in Ref. 3. These corrections remove the effects of gravity and spinner from the measured performance data.

The data reduction process for the pressure and airloads measurements is described in Ref. 2. The pressure coefficient is obtained from the pressure by dividing by the local section dynamic pressure: $c_p = p/(^1/_2\rho U^2)$,

where U is the local blade velocity obtain by combining free stream velocity and blade rotational velocity. The section normal force coefficient, $c_n = N/(^1/_2\rho U^2 c)$ is obtained by integrating the pressure coefficients.

## Test Conditions

Reference 3 reports that pressure data were acquired for 463 points consisting of 29 static points, 330 helicopter mode points, 37 airplane mode points, and 67 hover mode points. Reference 3 discusses the pressure instrumentation problems and how it affects the availability of obtaining section airloads from the chordwise pressure data at the seven radial locations.

Pressure data were acquired at advance ratios of 0.125, 0.15, 0.175, and 0.20; and at $C_T/\sigma$ of 0.089, 0.108, and 0.128 (some limited data acquired at 0.098 and 0.118). Multiple repeat points were acquired at each test condition. Some 98 different test conditions were identified and the availability of leading edge pressure data and section airloads was examined. Essentially, as the DNW test progressed, instrumentation problems prevented the determination of section airloads at several stations. Also blade leading edge transducers on either the upper or lower blade surface might have been non-operational for later test points.

Twelve test conditions were selected for this initial evaluation of the ability of linear regression models and neural networks to estimate the blade section normal force coefficient from a limited set of blade pressure data. These twelve test conditions are for helicopter mode forward flight and were analyzed in detail in Ref. 4. The nominal operating conditions are advance ratio $\mu = V/\Omega R = 0.15$, rotor thrust $C_T/\sigma = 0.089$ and 0.128, and shaft angle of attack from $-10^o$ (forward) to $+10^o$ (aft).

Sample blade section airloads measured in helicopter mode are presented in Figs. 1 and 2, which show $c_n$ as function of azimuth at the r/R = 0.90 and = 0.62 radial stations, respectively. The measured airloads show significant blade-vortex interaction at the tip for all twelve conditions, at both high and low thrust, and at both positive and negative shaft angles.

## Evaluation Database

The test conditions, the blade pressure data at the various chord-wise locations, and the blade section normal force coefficient data for seven radial stations, r/R, were combined into a single database upon which the linear regression and neural network computations

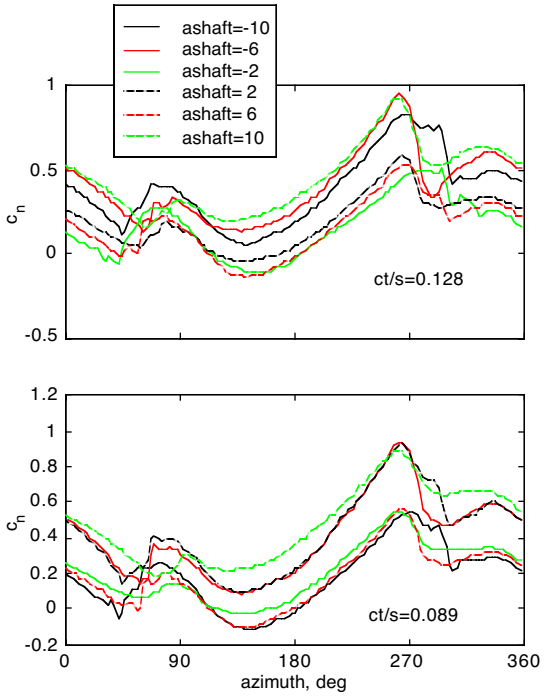


**Fig. 1. Measured TRAM helicopter mode airloads for μ = 0.15 at radial station r = 0.90R.**

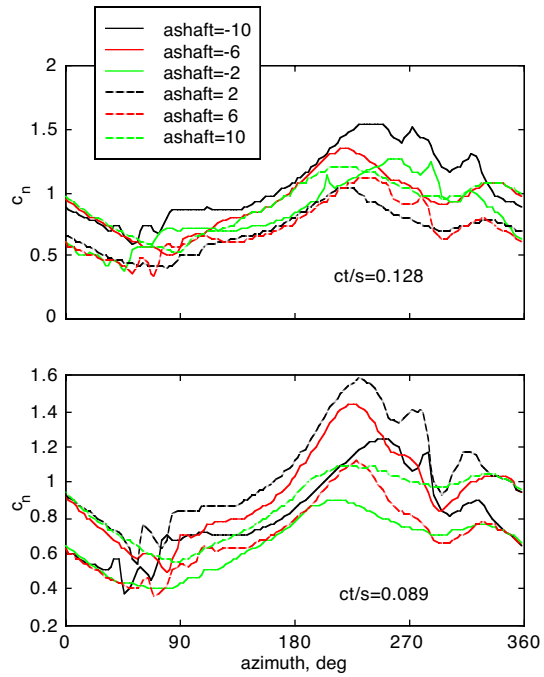


**Fig. 2. Measured TRAM helicopter mode airloads for μ = 0.15 at radial station r = 0.62R.**

were performed. The airloads could not be determined at all seven radial stations for all twelve test conditions due to instrumentation problems with pressure transducers at various blade stations. Such instrumentation problems were corrected to the extent possible between test runs. Therefore different pressure transducers were non-operational for different test points acquired at different times during the wind tunnel test.

Concatenating the data for the twelve test conditions results in 12*128=1536 samples for each measurement channel in the database. The database for this study contains 60 possible input channels (four test conditions, azimuth angle, and 45 blade leading-edge pressures from fourteen radial location r/R and acquired at the 2.0%, 3.5%, or 6.5% chord-wise station) and seven possible output channels ($c_n$ at r/R=0.96, 0.90, 0.82, 0.72, 0.62, 0.50, and 0.33).

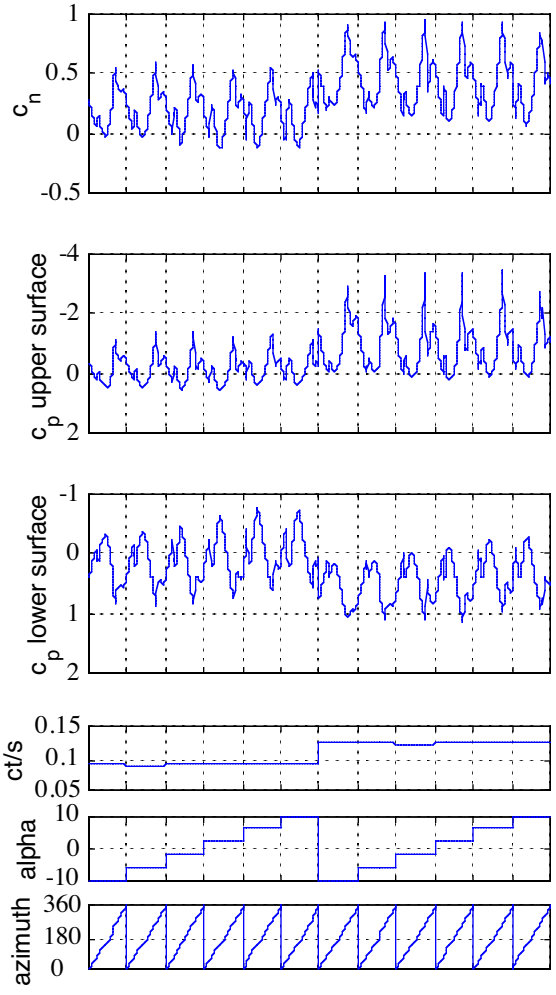


**Fig. 3. Airloads and blade leading-edge pressure measurements at 3.5% chord at radial location r/R=0.90 and test conditions.**

Figure 3 depicts the data base content for the airloads at r/R=0.90 and shows the $c_n$ data, the $c_p$ measurements at the 3.5% chord-wise location on the upper and lower blade surface, the test conditions $C_T/\sigma$ and shaft angle of attack, $\alpha$, and the azimuth angle, $\psi$. The additional test conditions, being advance ratio and tip Mach number at nominal values of 0.15 and 0.63, respectively, are essentially constant and are not plotted in Fig. 3. The vertical grid lines in Fig. 3 separate the twelve test points as can be clearly seen in the $\alpha$ and azimuth angle plots.

Figure 3 shows very similar trends in the airloads $c_n$ data and the leading-edge pressure data, $c_p$ on the blade upper surface.

Figure 4 graphically shows the relationship between section airloads and the pressures measured at the 3.5% chordwise location on the upper and lower blade surfaces for three radial locations (0.90R, 0.72R, and 0.62R). A non-linear trend is seen between $c_n$ and $c_p$,

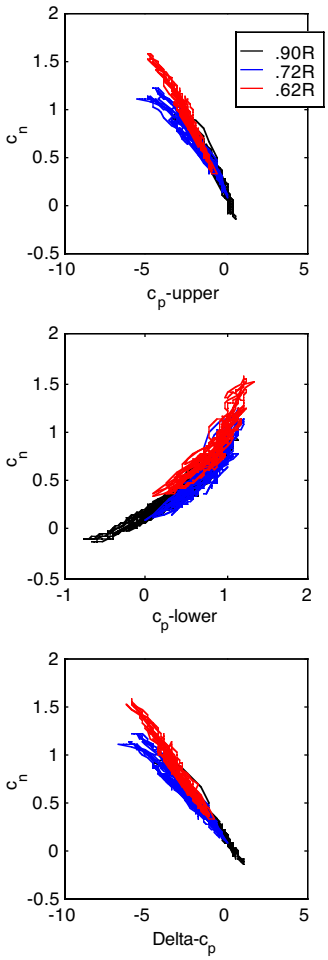


**Fig. 4. cn versus cp plots for upper and lower blade pressure measurements for three radial locations**

with the non-linearity being greater for the lower surface $c_p$ . Reduced non-linearity between $c_n$ and $c_p$ is seen for the more inboard locations. Also shown in Fig. 4 is $c_n$ as function of Delta_$c_p$=$c_{p,upper}$-$c_{p,lower}$, which shows a more linear trend, especially at the inboard locations.

### Mathematical Models

The use of linear regression analysis and of neural network analysis was investigated to estimate the blade section airloads from blade leading edge pressures and representative test conditions. The regression and neural network models are discussed next.

### Linear Regression Model

The general linear regression equation is:

$$c_{n,est} = a_0 + \Sigma\, a_{1,i}\, X_i + \Sigma\, a_{2,i}\, X_i^2 + \Sigma\, a_{3,i}\, X_i^3 + \ldots \quad (1)$$

where $c_{n,est}$ is the estimated blade section normal force, $X_i$ are the regression input variables, and $a_{j,i}$ are the regression coefficients.

The $X_i$-variables are: advance ratio $\mu$, shaft angle of attack $\alpha_{shaft}$, $C_T/\sigma$, tip Mach number, $M_{tip}$, and the blade leading-edge pressure measurements, $c_p$ at 2%, 3.5%, or 6.5% chord on the upper and lower blade surfaces at the considered radial station, r/R.

The general linear regression Eq. (1) includes higher order terms. However, only higher order terms for $c_{p,upper}$ and $c_{p,lower}$ are considered in this investigation. The test condition parameters are constant for a particular test point and are only incorporated as linear terms in the regression model.

### Neural Network Model

A two-layer neural network (nn) model as depicted in Fig. 5 was used in the present investigation to estimate the blade sectional normal force coefficient, $c_n$, from measured leading edge pressure measurements and test condition parameters. A number of two-layer networks were studied varying in the number of inputs and in the number and type of hidden layer nodes. A Levenberg-Marquardt scheme is used to train the networks.

Only multiple-inputs / single output (MISO) neural network models were considered for this investigation: a MISO-network for each radial location, r/R, for which the section normal force coefficient, $c_n$, is to be estimated.

The inputs to the neural network model consisted of the measured blade leading-edge pressure coefficient, $c_p$, (at 2%, 3.5%, or 6.5% chord) on the upper and lower blade surface, the azimuth angle, $\psi$, and the four test condition parameters, $\mu$, $M_{tip}$, $\alpha_{shaft}$, and $C_T/\sigma$. The output of the network was the estimated airloads data, $c_{n,est}$, at the radial station, r/R.

The number of nodes in the hidden layer was varied from 1 to 6. Tangent hyperbolic activation functions in the hidden layer were used without or with one linear activation function node. A linear transfer function and a tangent hyperbolic activation output function were considered for the output node. Initial work showed the linear transfer function in the output node to provide superior results and was therefore specified for the remainder of the investigation.

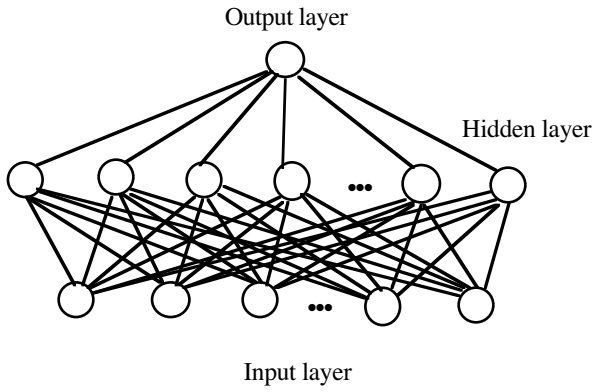


**Fig. 5. Schematic of a two-layer neural network perceptron (multiple inputs / single output)**

### Matlab® Toolbox

A Toolbox of Matlab® codes was developed by the author to perform the regression and nn-analyses using Matlab®, version 5.2, running on a MacIntosh PowerBook G4 (800 MHz, OS 9.2). Various neural network functions from Ref. 9 were incorporated in the Toolbox. The Toolbox user specifies by means of a Graphical User Interface (GUI) the database to be loaded, the desired analysis method (regression or neural network), the multiple inputs and single output to the model, and the analysis model structure. For the regression model, a GUI-popup window allows the user to specify for each selected input the order to which the input should be represented in the model (see Eq. 1). For the nn-option, the user specifies the network architecture; i.e. number/type of nodes in the hidden/output layer.

It should be noted that if a pressure transducer for a particular test condition was non-operational, the corresponding $c_p$ values were set to NaN (Not-A-Number) in the TRAM DNW blade pressure database. Similarly, if insufficient pressure measurements along the chord were available at a test condition to compute

the section normal force coefficient at a radial station, all corresponding $c_n$-values in the database for that test condition were set to zero. In performing the regression and neural network analysis for a particular r/R-location, these $c_p$=NaN and $c_n$=0 data are identified. The Toolbox allows for the elimination of such test points in the loaded database when estimating the regression coefficients or neural network nodal weights (training cycle). Also, the Toolbox allows for the creation of a training data set and a separate test data set for evaluating the math model.

The Toolbox also allows for the export and import of the neural network models (input/output selection, architecture and corresponding weight matrices) to allow for the evaluation of the networks in estimating airloads from different data subsets.

The Toolbox allows for the export and import of the airloads data in tabular format and for the depiction of such data in graph form so as to compare the results of the various linear regression math models and various neural network models.

The stopping criteria for training the neural network is either to achieve an error bound tolerance for two consecutive epochs of $10^{-12}$, or to exceed 1000 training epochs. Typically the limit of 1000 epochs terminates the network training for networks containing more than 3 to 4 nodes in the hidden layer.

## Analysis Approach

The number and the type of inputs to the regression model of Eq. (1) and to a specific neural network architectural model (Fig. 5) are systematically varied to evaluate their contribution to accurately estimate the blade section normal force coefficient.

The measured and estimated $c_n$ data are graphically displayed by the Toolbox as are the residual error data given by $c_n$-$c_{n,est}$. Figure 6 presents an example of this graphical display, showing the measured versus estimated data in the top plot and the residual error data in the bottom plot. The estimated airloads in Fig. 6 represent the results of a linear regression analysis model using only the blade upper surface $c_p$-data at 3.5% chord to estimate the $c_n$-data at r/R=0.90. As indicated by the x-axis label, the vertical dotted lines in Fig. 6 separate the database subsets, i.e. the airloads over one azimuth sweep for each of the twelve considered test conditions. The measured and estimated airloads as well as the residual error data for subset seven ($\alpha$=-10°, $c_T/\sigma$=0.128) are presented in Fig. 7 to show more detail. Although the general trend of $c_n$ as a function of the azimuth angle is captured by the math model as shown in Fig. 7, the magnitude of the airloads estimate is fairly inaccurate.

The Toolbox also allows for conversion of $c_p$ and $c_n$ to $c_pM^2$ and $c_nM^2$, respectively, where M is the local blade section Mach number obtained from

$$M = [(V\sin\psi\ \cos\alpha_{shaft}+\Omega r)^2+(V\sin\alpha_{shaft})^2]/a^2 \qquad (2)$$

This Toolbox conversion option allows for the evaluation of the ability of the regression and neural network models to also estimate airloads in terms of $c_nM^2$ from blade pressure data expressed as $c_p$ or $c_pM^2$. Figure 8 shows an example of the measured and estimated $c_nM^2$ data at 0.90R using a regression model with $c_pM^2$, measured at 3.5% chord on the blade upper surface as the sole input. Figure 9 shows the corresponding data from the seventh subset ($\alpha$=-10°, $c_T/\sigma$=0.128).

The standard deviation (S.D.) of the residual error data is shown in the upper-right corner in the residual error plots of Figs. 6 and 8. The standard deviation of the residual error data is used as a metric of the "goodness" of fit of the airloads prediction. This metric facilitates the comparison of the various regression and neural network models in their ability to accurately estimate the airloads.

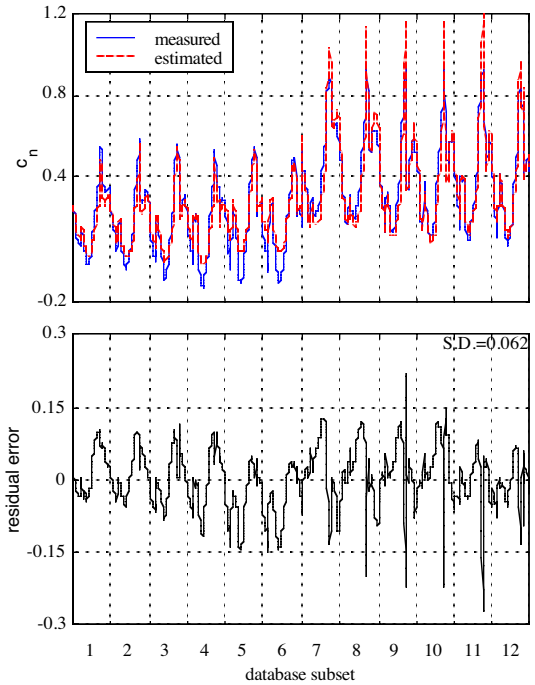


**Fig. 6. Sample plots of measured versus estimated airloads from regression model (input: $c_{p,3.5}$) and of residual error plot (input $c_{p,upper}$-data at 3.5%c; r/R=0.90)**

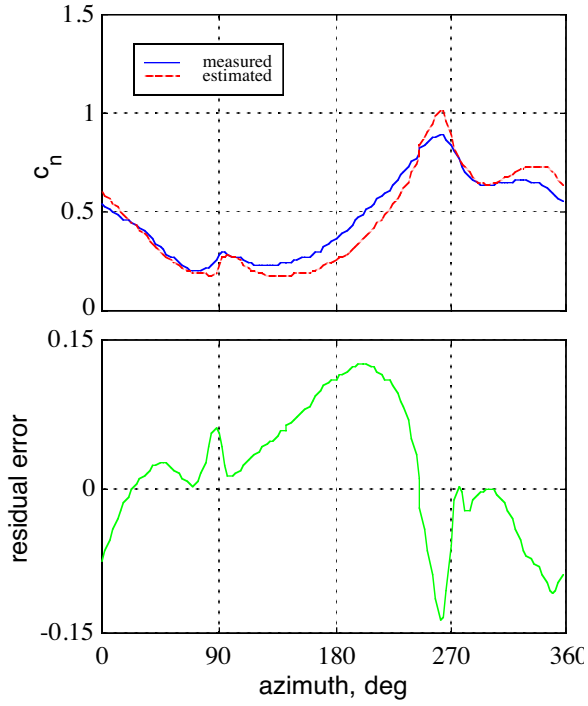


**Fig. 7. Measured versus estimated airloadfrom regression model (input: $c_{p,3.5}$) and residual error as function of azimuth angle for database subset #7 of figure 6 ($\alpha$=–10°, $c_T/\sigma$=0.128)**

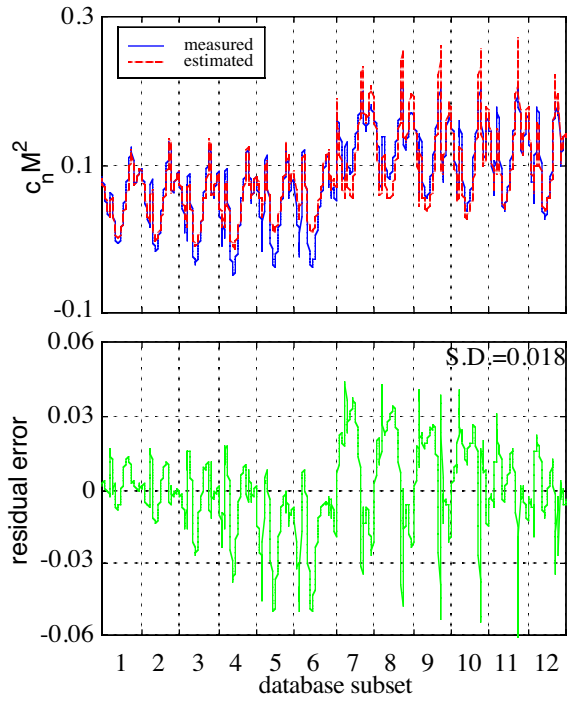


**Fig. 8. Sample plots of measured versus estimated airloads from regression model (input: $c_{p,3.5}M^2$) expressed as $c_nM^2$ and residual error (input: $c_{p,upper}$-data at 3.5%c; r/R=0.90)**

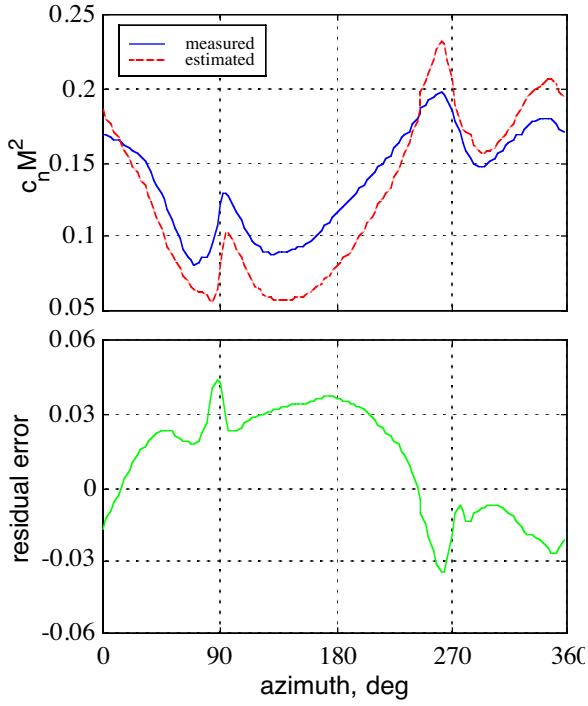


**Fig. 9. Measured versus estimated airloads from regression model (input: $c_{p,3.5}M^2$) expressed as $c_nM^2$ and residual error as function of azimuth angle for database subset #7 of figure 8 ($\alpha$=-10°, $C_T/\sigma$=0.128)**

### Regression model evaluation

The upper and lower surface pressure measurements at the 3.5% chordwise stations in combination with the various test conditions and azimuth angle were used as inputs to various regression models to estimate the blade section normal force coefficient, $c_n$. Figure 10 shows the goodness of fit when assuming only linear terms in Eq. 1 and varying the inputs to the regression model. The standard deviation of the residual error in the airloads estimation, being the goodness of fit of the considered model, is shown along the x-axis in Fig. 10. The various inputs to the considered regression models are shown along the vertical axis of Fig. 10.

Figure 10 shows that using only the upper surface $c_{p,\ upper}$ data provides better load estimations than using only the lower surface $c_{p,\ lower}$ data. This is especially true for the more inboard locations. Using both upper and lower surface pressure data improves the airloads estimation at all radial locations. Including the test conditions gives only minor improvements in the airloads estimation.

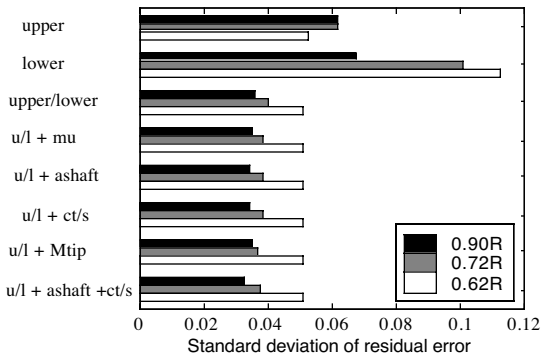


**Fig. 10. Goodness of fit for $c_n$ regression models with various inputs and assuming linear trends**

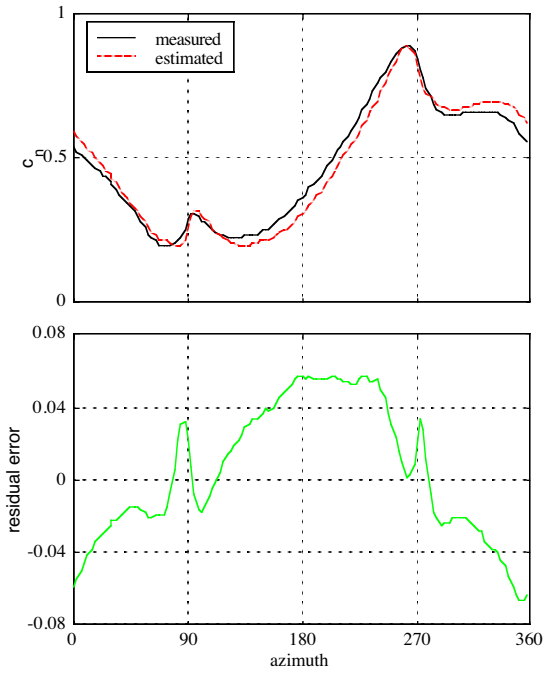


**Fig. 11. Measured versus estimated airloads from regression model (input: $c_{p,upper,3.5}$, $c_{p,lower,3.5}$, $\alpha$, $C_T/\sigma$) expressed as $c_n$ and residual error as function of azimuth angle for database subset #7 ($\alpha$=-10°, $C_T/\sigma$=0.128)**

Figure 7 shows a representative example (subset #7: $\alpha$=-10°, $C_T/\sigma$=0.128) of the airloads estimation for 0.90R when only the upper surface pressure is an input to the regression model. The overall goodness of fit for this regression model is shown as the top bar (labeled 'upper') in Fig. 10 for 0.90R. Figure 11 shows the estimation for the same data subset #7, but for the regression model which has as inputs $\alpha$, $C_T/\sigma$, and the upper and lower surface pressures at 3.5% chord. The overall results for this regression model are depicted in Fig. 10 as the bottom bar (labeled 'u/l + ashaft + ct/s') for 0.90R. The improvement seen in the airloads estimation when comparing Figs. 7 and 11 is mostly due to including the lower blade surface pressure as input to the regression model.

Figure 4 shows a non-linear trend between airloads and blade leading edge pressures. Therefore, including higher order pressure terms in the regression model was investigated (see Fig. 12). The test conditions were maintained as first order terms only. Figure 12 shows that including second order pressure terms improves the load estimation essentially only when the upper surface pressure is the sole input to the regression model and its influence is reduced substantially for the more inboard radial locations.

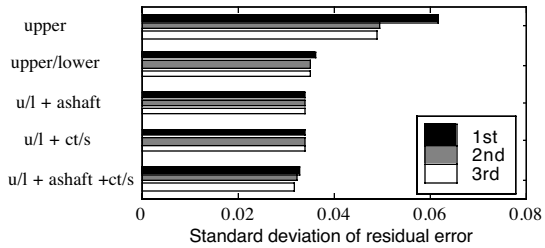


a. 0.90R

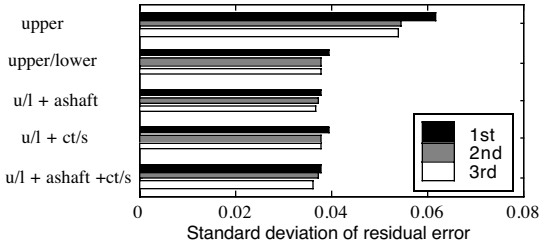


b. 0.72R

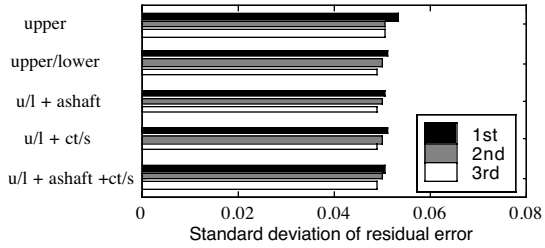


c. 0.62R

**Fig. 12. Goodness of fit for $c_n$ regression models, incorporating higher order terms for pressure data at three radial locations**

Regression analysis models in which $c_pM^2$-data are inputs and $c_nM^2$-data are the output were also evaluated. Figure 13 shows representative results at the 0.90R radial location. Again the inclusion of the second order

pressure terms shows the largest effect if $c_{p,upper}$ is the sole input to the model. The results show that the second order term's contribution to improving the accuracy of the $c_nM^2$ prediction diminishes for the more inboard locations. A comparison of Figs. 12a and 13 shows that the influence of $C_T/\sigma$ is much greater when estimating airloads in terms of $c_nM^2$ versus $c_n$ at the 0.90R stations. For the 0.72R and 0.62R stations minimal improvements in $c_nM^2$ estimation are seen from the inclusion of $C_T/\sigma$ as an input.

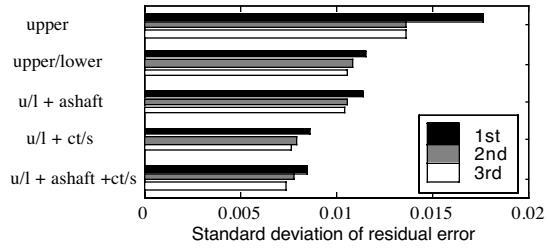


**Fig. 13. Goodness of fit for $c_nM^2$ regression models for 0.90R, incorporating higher order terms for pressure data**

Figure 9 shows a representative sample of a regression model to estimate the airloads in the format $c_nM^2$ (subset #7, $\alpha$=-10°, $C_T/\sigma$=0.128) when using only upper surface pressure, $c_pM^2$, as an input. Figure 14 shows the same subset, but for the regression model, which has as inputs $\alpha$, $C_T/\sigma$, and the upper and lower surface pressures, $c_pM^2$, at 3.5% chord. The overall goodness of fit for the database for these two regression models is shown in Fig. 13 as the 1st order models with y-axis labels of 'upper' and 'u/l + ashaft + ct/s', respectively. Most of the improvement in the airloads estimation between Figs. 9 and 14 is due to the inclusion of the lower surface pressure as an input to the regression model.

### Neural network model evaluation

Figures 15 through 17 summarize the results of varying the inputs to various neural network models in estimating the airloads, $c_n$, at radial locations 0.90R, 0.72R, and 0.62R, respectively. The evaluation metric, the standard deviation of the residual error, is shown along the x-axis in Figs. 15-17. The model input description is provided in the y-axis of the subplots of Figs. 15-17. Seven input scenarios are considered as shown along the y-axis. The model inputs are the upper (u) or lower (l) blade pressure measurements at 3.5%-chordwise station as single inputs and as combined inputs, as well as these two pressure measurements in combination with the test parameters of shaft angle of attack (ashaft) and thrust level (ct/s).

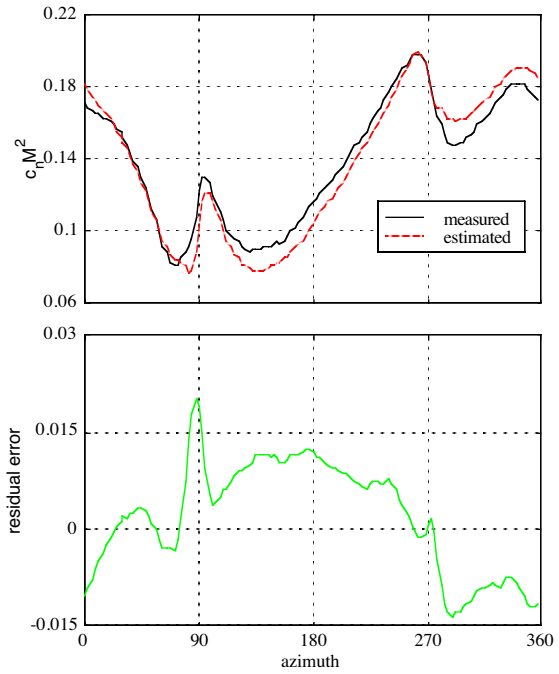


**Fig. 14. Measured versus estimated airloads from regression model (input: $c_{p,upper,3.5}M^2$, $c_{p,lower,3.55}M^2$, $\alpha$, $C_T/\sigma$) expressed as $c_nM^2$ and residual error as function of azimuth angle for database subset #7 ($\alpha$=-10°, $C_T/\sigma$=0.128)**

The azimuth angle (label=az) is also considered as an input. The five input case consists of upper and lower blade pressures and $\alpha$, $C_T/\sigma$, and $\psi$. The upper and lower blade pressure measurements were considered as individual inputs as both pressures were not always available for each test points at all radial locations (see Table 1). Advance ratio and tip Mach number were also considered as inputs. However, since these test parameters varied only slightly for the twelve considered test cases, inclusion of these parameters as nn-input showed negligible effect on the accuracy of the airloads estimation.

The neural network model's architecture is defined in the legend of each subplot of Figs. 15-17. The following nomenclature is used to identify these networks. The letter 'L' is used to identify a linear node in the hidden layer, whereas 'H' is used to identify a tangent hyperbolic activation function for a node in the hidden layer. The number 'i' in 'LHi' or 'Hi' identifies the number of such H-functions in the hidden layer. Only one linear node is considered for the hidden layer. The output layer has a linear activation function. Thus the LH4 network contains one linear node and four nodes with tangent hyperbolic activation functions in the hidden layer and has a linear output node. Twelve such

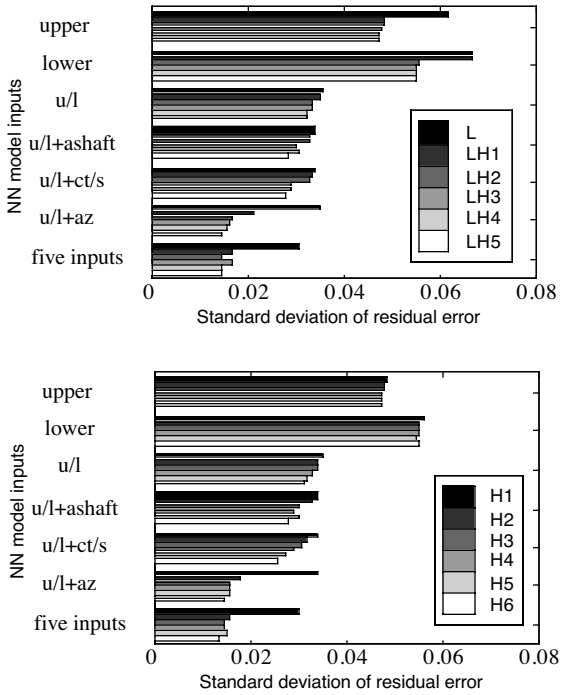


**Fig. 15. Goodness of fit for neural network models in estimating airloads $c_n$ at radial station 0.90R using various inputs (pressures at 3.5% chord)**

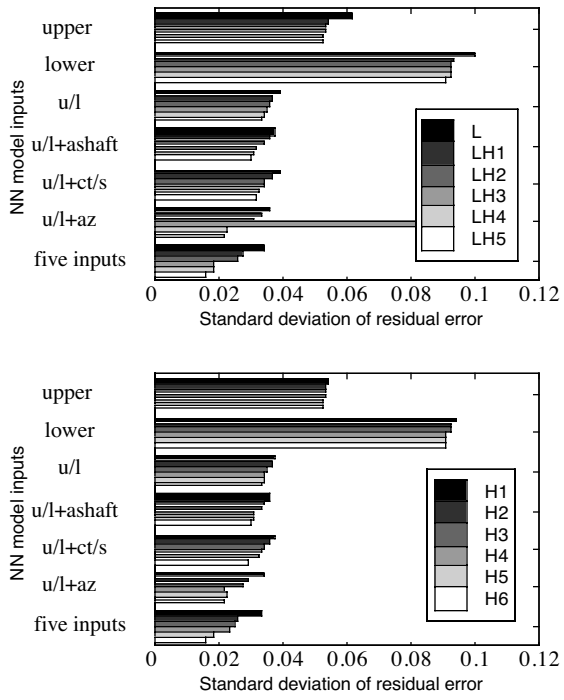


**Fig. 16. Goodness of fit for LHi neural network models in estimating airloads $c_n$ at radial station 0.72R using various inputs (pressures at 3.5% chord)**

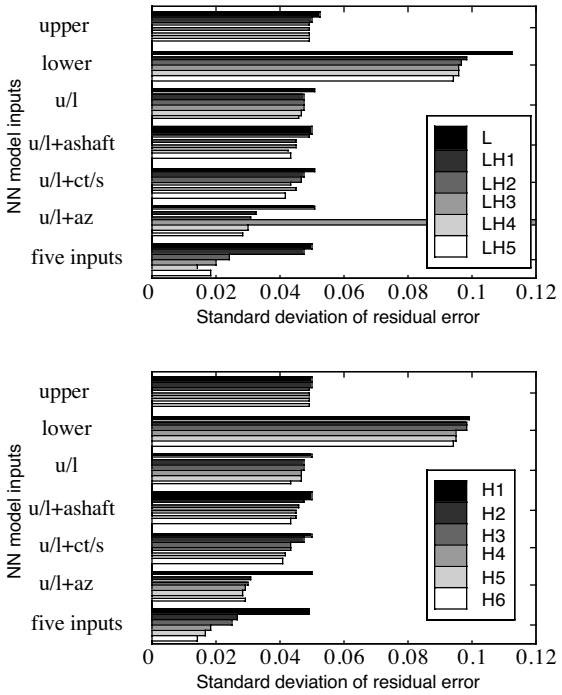


**Fig. 17. Goodness of fit for neural network models in estimating airloads $c_n$ at radial station 0.62R using various inputs (pressures at 3.5% chord)**

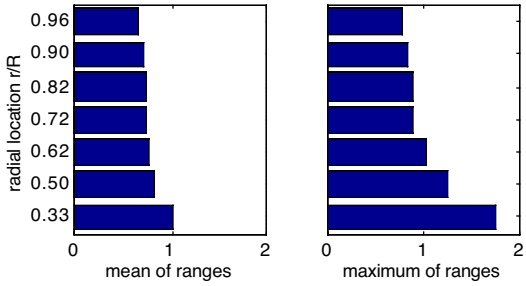


**Fig. 18. Mean of ranges and maximum range of airloads $c_n$ for considered test points for seven radial locations**

neural network configurations were considered having from 1 to 6 nodes in the hidden layer and containing one or no linear activation function in the hidden layer (see Figs. 15–17).

It should be noted that a neural network having just one linear node in the hidden layer and a linear output node will essentially provide the linear regression model results in which all inputs are represented as linear terms only. The regression coefficients can be derived from the weights obtained in this 'L' neural network model.

When comparing the goodness of fit metric from airloads estimations at different radial stations it needs to be kept in mind that the magnitude of the mean and the range of airloads changes with the radial location. The range of the airloads, defined as maximum – minimum, for each test point was determined and the mean of these ranges as well as the maximum range are shown in Fig. 18. Note that both the mean and maximum range increases as r/R decreases.

Figure 15 shows that for a specific neural network model architecture (L, LH, etc), using only the upper surface blade pressure gives better airloads estimates as compared to using only the lower surface blade pressure which was expected from the trends observed in Figs. 3 and 4 and from the linear regression results. The estimation of the airloads from the lower blade surface pressure becomes less accurate as a more inboard radial location is considered (Figs. 16–17). Improvement in the airloads estimation is seen when both upper and lower blade surface pressures are used, although this improvement over the upper-surface pressure-only case is minimal for the 0.62R radial location (Fig. 17).

Inclusion of test conditions $\alpha$ and $C_T/\sigma$ as model input parameters tends to improve the airloads estimation of the nn-models with more than two-three nodes.

Note the improvement that is seen in Figs. 15–17 in the nn-models by including the azimuth angle (az) as an input parameter. This improvement with be discussed in more detail when describing the airloads estimation results in terms of $c_nM^2$.

For a given input set, increasing the number of nodes in the neural network's hidden layer tends to improve the airload estimation accuracy (Figs 15-17). The initial improvement when going from a one node 'L' network to a two node 'LH' network is substantial for the 0.90R station (Fig. 15) when only the upper or the lower $c_p$ pressure is an input to the network. Substantial improvements for all three radial locations are also seen for the five-input cases when adding nodes to the hidden layer (Figs 15-17).

Figures 15-17 show that a one-node 'H' network performs better than a one-node 'L' network. However, as more nodes are added, the LHi and Hi networks tend to perform equally well in estimating the airloads, $c_n$.

Figures 19 through 21 show the analysis results using the same neural network model architectures, but using as inputs the upper and lower blade pressure measurements at 3.5%-chordwise station in the form of $c_pM^2$ and the output parameter being $c_nM^2$. Figure 22 shows the mean and the maximum of the ranges of the $c_nM^2$ airloads. Note that both the mean and maximum values decrease as r/R decreases.

Similar observations can be made for the $c_nM^2$ goodness fit in Figs. 19-21 as previously made for the $c_n$-airloads estimation (Figs. 15-17): adding nn-nodes for a specific input set tends to improve the estimation; a substantial improvement is seen when going from a L to an LH model, especially at the 0.90R station; the additional input of $\alpha$ or $C_T/\sigma$ improves the fit; using upper and lower surface pressure inputs provides better estimations as compared to inputting only the upper or lower surface pressure; and upper surface pressure only provides better estimates as compared to lower surface pressure only, especially at the inboard radial stations. At 0.90R the addition of $C_T/\sigma$ in Fig. 19 shows substantial improvements in the $c_nM^2$ estimation, which were not observed in Fig. 15 in estimating $c_n$.

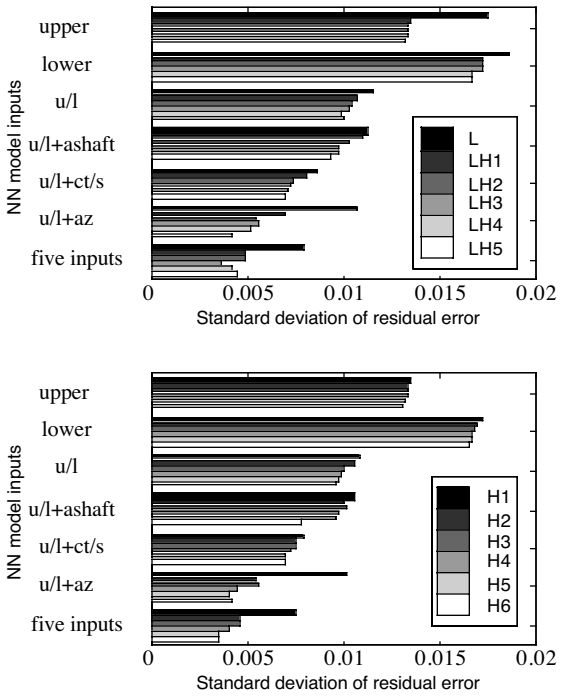


**Fig. 19. Goodness of fit for neural network models in estimating airloads $c_nM^2$ at radial station 0.90R using various inputs (pressures at 3.5% chord)**

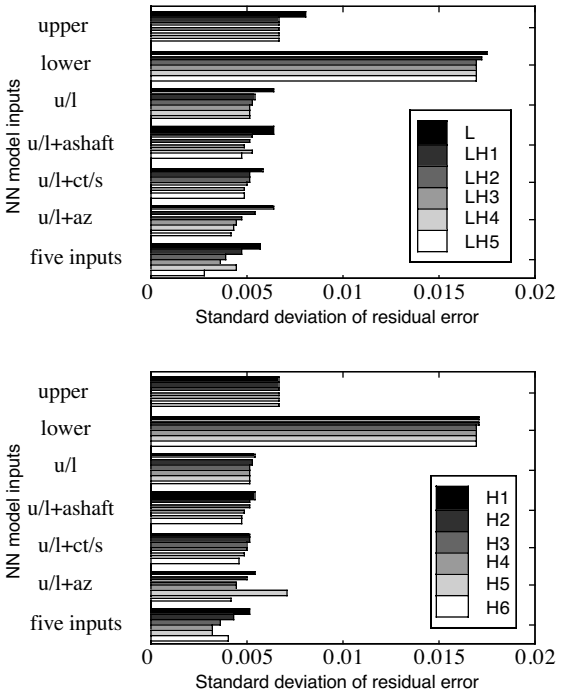


**Fig. 20. Goodness of fit for neural network models in estimating airloads $c_nM^2$ at radial station 0.72R using various inputs (pressures at 3.5% chord)**

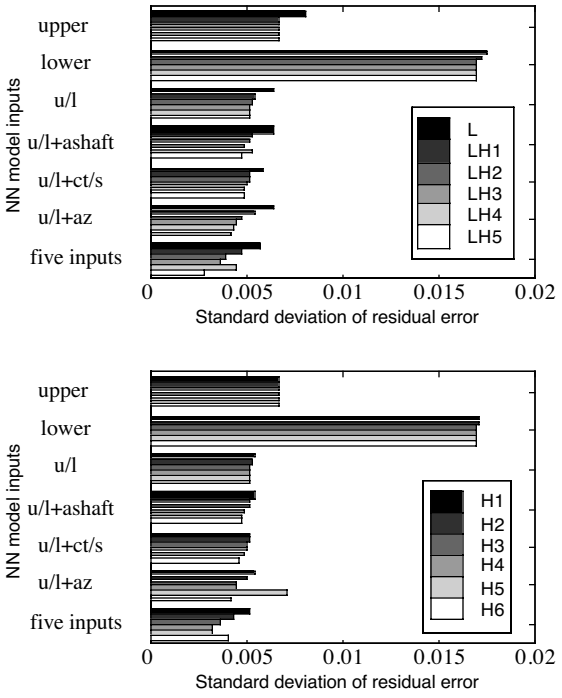


**Fig. 21. Goodness of fit for neural network models in estimating airloads $c_nM^2$ at radial station 0.62R using various inputs (pressures at 3.5% chord)**

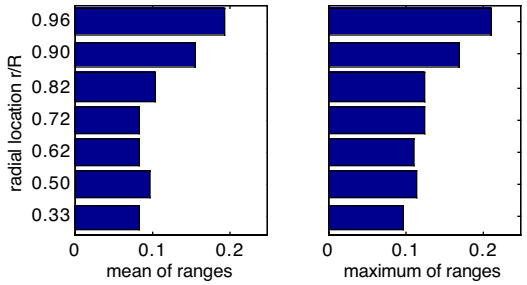


**Fig. 22. Mean of ranges and maximum range of airloads $c_n$ for considered test points for seven radial locations**

### Azimuth angle effect

The estimation of the airloads in terms of $c_n$ (Figs. 15-17) or $c_nM^2$ (Figs. 19-21) is improved by the input of azimuth angle to the neural network models. The influence of the azimuth angle input on the estimation accuracy of the airloads $c_nM^2$ is illustrated in Fig. 21, which shows the results of the LH3 neural network at the 0.90R radial station using as inputs $\alpha$, $C_T/\sigma$, and $c_p$-data on the upper and lower blade surface at the 3.5% chordwise station. Shown in Fig. 23 is the data subset for $\alpha$=-10° and $C_T/\sigma$=0.128. Reference 7 states that in attached flow, $c_n$ leads the $c_{p,2\%}$ data and describes a correction method

$$c_n = c_{n,\text{look-up-table}} + T_p \dot{c}_{n,\text{look-up-table}}$$

where in hovering flight the time constant, $T_p$, represents 10° at 0.5R and 5° at the tip. Providing the azimuth angle information to the neural network model results in the airloads estimation curve to move to the left in Fig. 23; i.e., it corrects for the $c_n$ leading $c_p$. This azimuth correction is seen at all radial locations. This correction is also seen when inputting only the upper or the lower blade surface pressure to the nn-model.

Although the azimuth does improve the nn-model airloads estimation, a problem was identified with this input in that the estimated airloads trace at 0° and 360° azimuth did not always line up correctly. This phenomenon is barely noticeable in Fig. 23 in the residual error plot. Presently the azimuth input is the saw-tooth trace seen in Fig. 3. Limited work was performed with an alternate azimuth input (sin(ψ), cos(ψ)) in an attempt to alleviate this phenomenon, but no consistent results were obtained. Future work will examine the substitution of a $\dot{c}_p$-type input for azimuth on the neural network's airloads estimation accuracy.

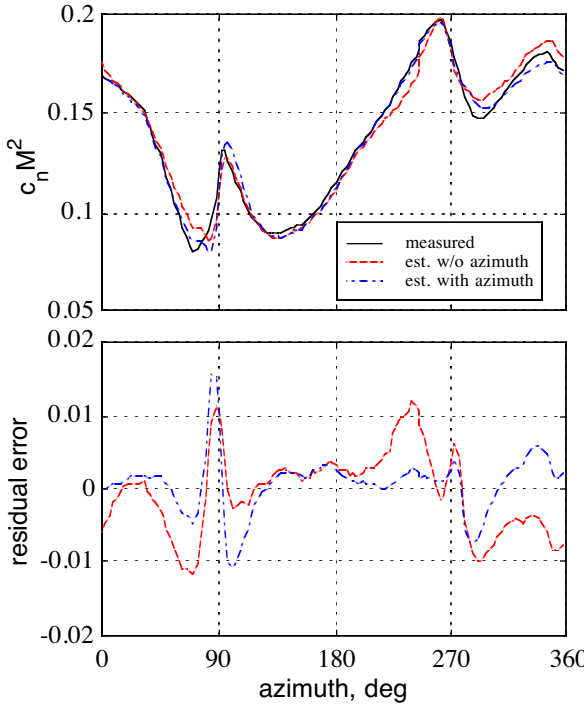


**Fig. 23. Measured versus estimated airloads (LH3-nn-model; without and with azimuth angle as input) and residual error as function of azimuth angle for database subset #7 ($\alpha$=-10°, $C_T/\sigma$=0.128)**

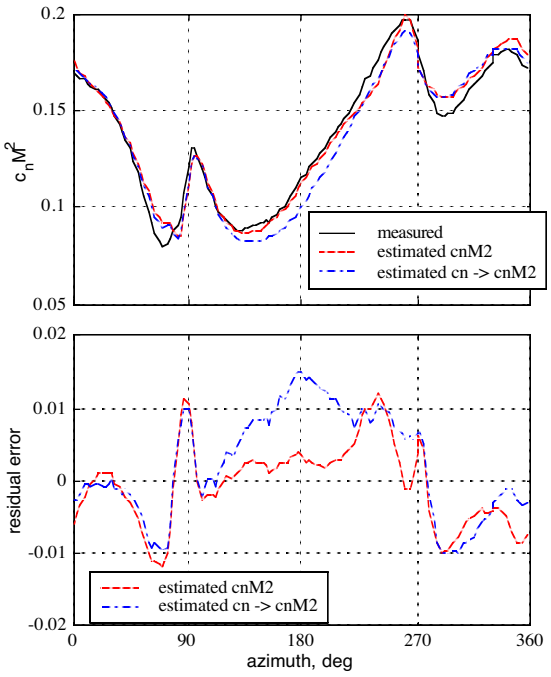


**Fig. 24. Measured versus estimated airloads $c_nM^2$ (LH3-nn-model without azimuth angle input) and residual error as function of azimuth angle for database subset #7 (0.90R, $\alpha$=-10°, $C_T/\sigma$=0.128)**

### $c_n$ versus $c_nM^2$ Airloads Estimation

Airloads estimation in the form of $c_n$ and $c_nM^2$ were obtained from various neural network models using as inputs $c_p$ and $c_pM^2$ at 3.5% chord, respectively. The estimated $c_n$-data form the LH3-model were converted to $c_nM^2$ and compared to measured $c_nM^2$-data and the estimated $c_nM^2$ obtained from the LH3-model using $c_pM^2$-data as input and measured $c_nM^2$-data as output. Additional nn-inputs are $\alpha$ and $C_T/\sigma$, while azimuth is an option input. Figures 24 and 25 compare the measured $c_nM^2$ airloads for 0.90R at $\alpha$=-10° and $C_T/\sigma$=0.128 with the directly estimated $c_nM^2$ airloads and after conversion of the estimated $c_n$-airloads to the $c_nM^2$-format. Figure 24 presents nn-results without azimuth input, whereas the results of Fig. 25 are for the nn-model, which has azimuth as an input. Figure 24 shows that largest difference in the $c_nM^2$–estimates occur for azimuth angles from 100° to 220°. In this region more accurate results are obtained from a nn-model, which computes $c_nM^2$ directly as compared to a nn-model, which estimates $c_n$ first. Figure 25 shows that the differences in airloads estimates from the two nn-models become small when azimuth is an nn-input.

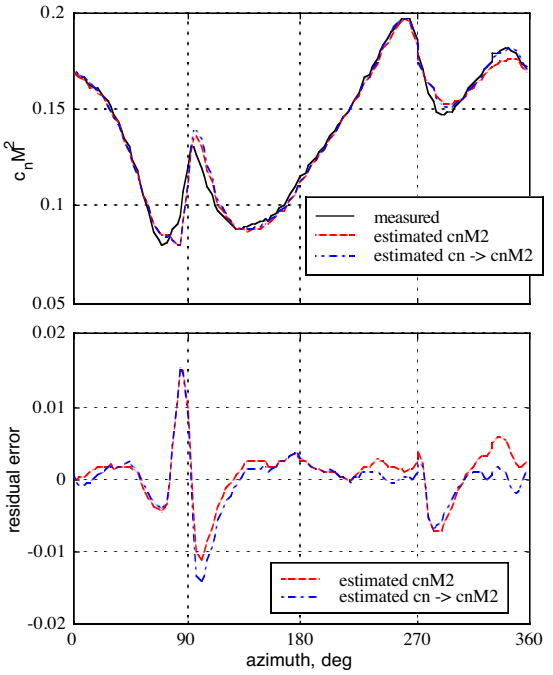


**Fig. 25. Measured versus estimated airloads $c_nM^2$ (LH3-nn-model with azimuth angle input) and residual error as function of azimuth angle for database-subset #7 (0.90R, $\alpha$=-10°, $C_T/\sigma$=0.128)**

Review of the airloads traces for the twelve test conditions and for the various radial locations shows $c_nM^2$ being more accurately estimated from training a nn-model against $c_nM^2$ as compared to training the nn-model against $c_n$ for r/R=0.90, 0.82, and 0.72; the reverse is true for r/R=0.62. As seen in Figs. 24 and 25, the differences tend to be small, especially if azimuth is an nn-input.

### Influence of Leading Edge Pressure Transducer Location

Initial work in estimating the blade section airloads used the 3.5% chordwise station pressures since this is the only station at which pressure transducers were installed at the intermediate radial locations (r/R=0.98, 0.93, 0.87, 0.77, 0.67, 0.56, and 0.42; see Table 1). However, for the seven radial stations where detailed chordwise pressures are available, the pressure data from a different chordwise station can be selected as an nn-input. This might be a necessity if the 3.5% pressure transducer was non-operational. Figure 26 shows the effect of selecting pressures from different chordwise stations (2.0%, 3.5%, or 6.5% chord) as input to the network on the goodness of fit in estimating the airloads $c_nM^2$ at seven radial locations, which are identified in the y-axis label. The shaft angle, $\alpha$, and thrust, $C_T/\sigma$, are nn-inputs as well. Only the upper surface $c_pM^2$ data were used as input since the corresponding lower surface $c_pM^2$-data were unavailable in quite a few cases. Figure 26 shows the results of the LHi-neural network models, which are identified along the y-axis in each subplot. Results for the Hi-nn-models are similar, except that the H and H2 networks tend to provide better results than the L and LH networks.

Figure 26 shows that increasing the number of nodes in the neural network tends to improve the airloads estimation. At the 0.96R location, the 2.0% chordwise pressure provides improved airloads estimation as compared to more aft located pressure data; this is especially true for three or more nodes in hidden layer of the network model. For the 0.82R location the 2.0% pressure data provides less accurate airloads estimates as compared to the 3.5% and 6.5% chordwise pressure data and the 2.0% model-estimate accuracy decreases greatly for the more radial inboard stations.

Figure 26 shows slightly better estimates using the 3.5% chordwise pressure as compared to the 6.5% chordwise pressures for radial locations r/R=0.82, 0.72, and 0.50. The 6.5%-model is more accurate at r/R=0.62. Except for the most outboard radial stations, the 3.5%-chordwise station is an appropriate location for obtaining upper-surface leading-edge pressures from which blade section airloads can be estimated.

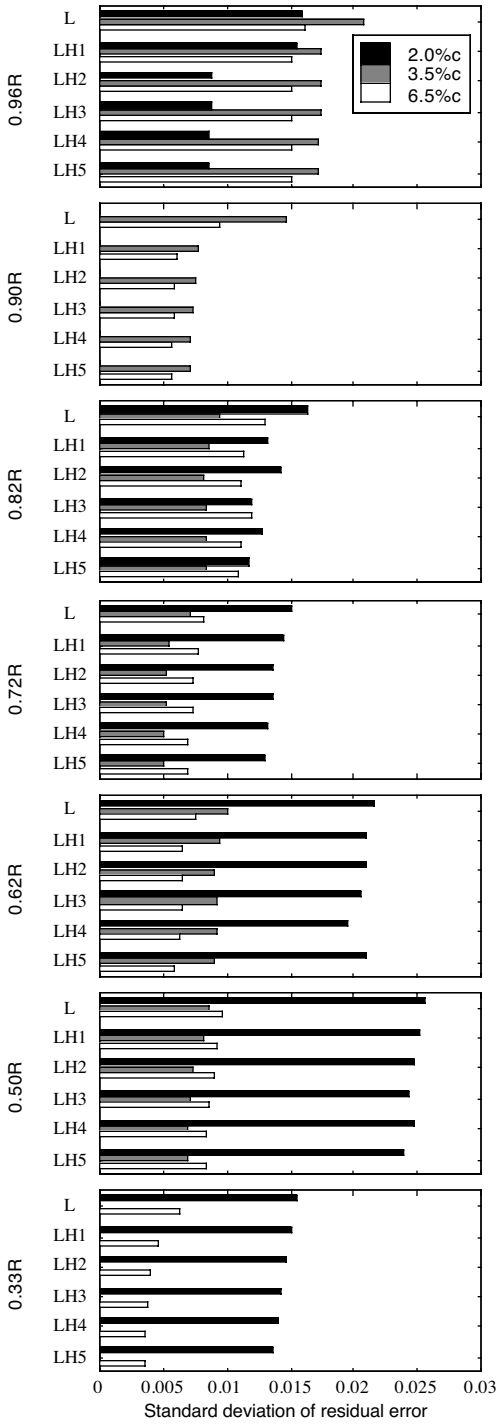


**Fig. 26. Goodness of fit for various LHi neural network models in estimating airloads $c_nM^2$ at seven radial stations (inputs: upper surface pressures at 2%, 3.5%, or 6.5% chordwise station, $\alpha$, and $C_T/\sigma$)**

Figure 27 shows the goodness of fit results for radial locations 0.90R and 0.62R for neural networks with both upper and lower surface pressures as inputs. Figure 27 shows again that the 2.0%-chordwise pressures provide more accurate results as compared to the 3.5%-c pressures at 0.96R. The 6.5%-chordwise pressures provide the most accurate results at 0.62R, while the 2.0%c and 3.5%c pressure provide similar goodness of fit results. Comparison of the corresponding subplots of Figs. 26 and 27 shows again that considerable improvement in the airloads estimation can be obtained if both the upper and lower surface pressures are input to the neural network model.

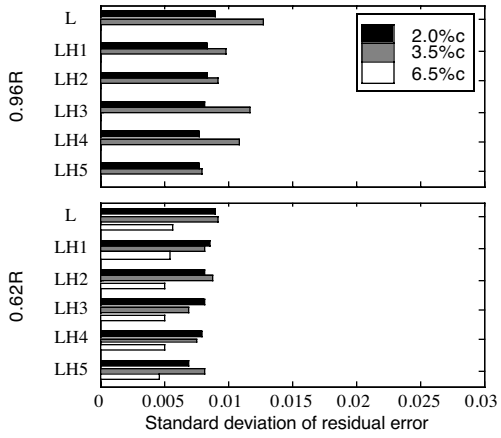


**Fig. 27. Goodness of fit for various LHi neural network models in estimating airloads $c_nM^2$ at two radial stations (inputs: upper/lower surface pressures at 2%, 3.5%, or 6.5% chordwise station, α, and $C_T/\sigma$)**

### Airload Estimation for Test Conditions Not Part of Training Database

The above discussion shows that neural networks with three or more nodes in the hidden layer do an adequate job in estimating the airloads from leading edge pressures for the training database. Such neural networks might be used to estimate the airloads for those test conditions where insufficient chordwise pressure data in the TRAM DNW-pressure database prevented the integration of pressures into the blade section airloads. To evaluate this ability, the $\alpha$=-10° test points were removed from the training data base for the 0.90R radial station and a LH3 neural network (inputs: $\alpha$, $C_T/\sigma$, and $c_pM^2$ at 3.5% chord, without and with azimuth) was trained against $c_nM^2$ from the remaining ten test conditions. The resulting two nn-models were subsequently used to estimate the airloads for the $\alpha$=–10° cases. Figures 28 and 29 show measured and estimated airloads for $\alpha$=-10° at $C_T/\sigma$=0.089 and $C_T/\sigma$=0.128, respectively. The airloads are estimated to within anticipated accuracy at both $C_T/\sigma$ levels. Note that the airloads traces for the nn-models with azimuth input do not line up at the 0° and 360° in the residual error plots of Figs. 28 and 29.

The ability of a LH3-model to estimate airloads for test points that are not part of the training database for the 0.62R radial station is shown in Figs. 30 and 31 for subsets 3 ($\alpha$=-2°, $C_T/\sigma$=0.089) and 10 ($\alpha$=+2°, $C_T/\sigma$=0.128), respectively. Figures 30a and 31a show the measured and estimated airloads when these two test points are part of the training database, whereas Figs. 30b and 31b show the estimates when these test points are not part of the training database. Comparison of the airloads estimates in Figs. 30a and 30b and in Figs. 31a and 31b for the 0.62R station and of Figs. 23 and 29 for the 0.90R station shows that the nn-models can be used successfully to estimate airloads for test conditions that were not part of the training database.

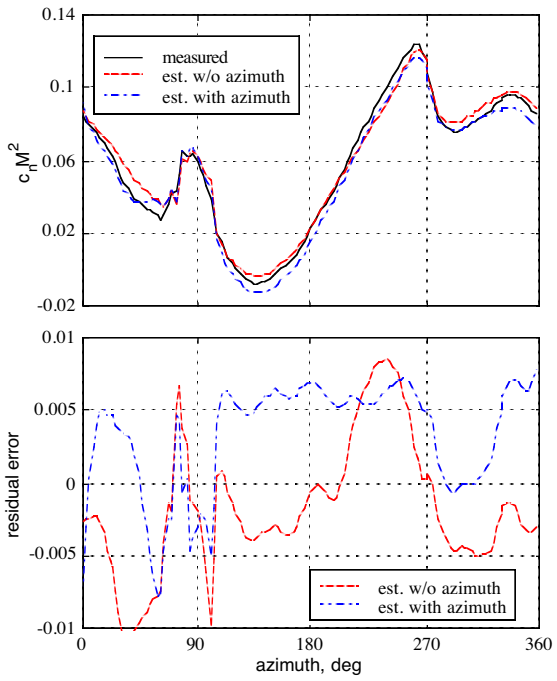


**Fig. 28. Measured versus estimated airloads (LH3-nn-model; without and with azimuth angle as input) and residual error as function of azimuth angle for database subset #1 (0.90R, α=-10°, $c_T/\sigma$=0.089); subsets #1 and #7 removed from training database**

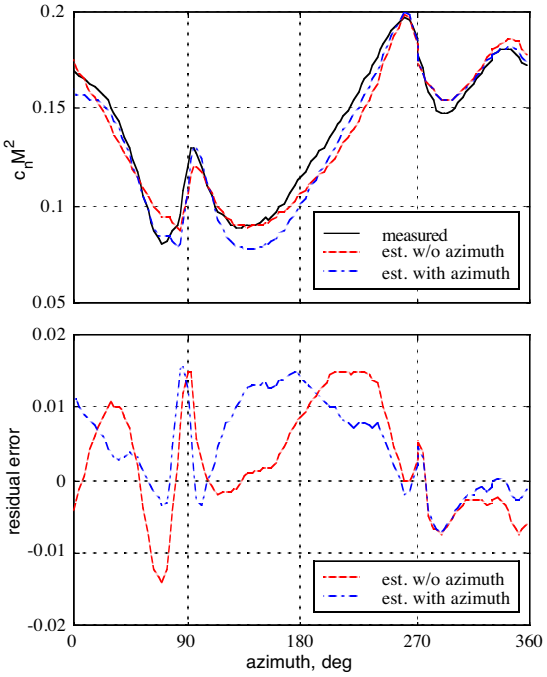


**Fig. 29. Measured versus estimated airloads (LH3-nn-model; without and with azimuth angle as input) and residual error as function of azimuth angle for database subset #7 (0.90R, $\alpha$=-10°, $c_T/\sigma$=0.128); subsets #1 and #7 removed from training database**

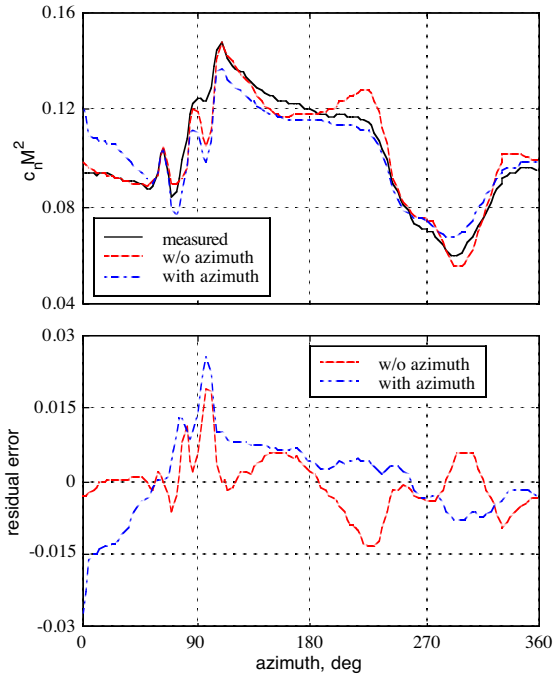


**a: subset is part of training set**

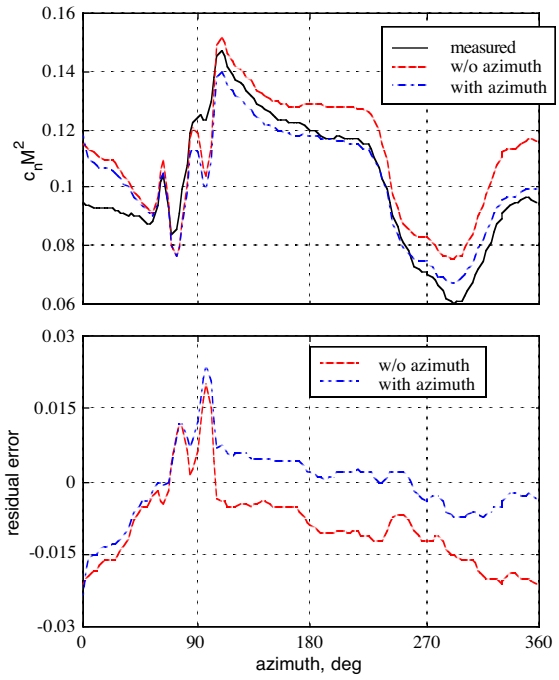


**b: subset is not part of training set**

**Fig. 30. Measured versus estimated airloads (LH3-nn-model; without and with azimuth angle as input) and residual error as function of azimuth angle for database subset #3 (0.62R, $\alpha$=-2°, $c_T/\sigma$=0.089)**

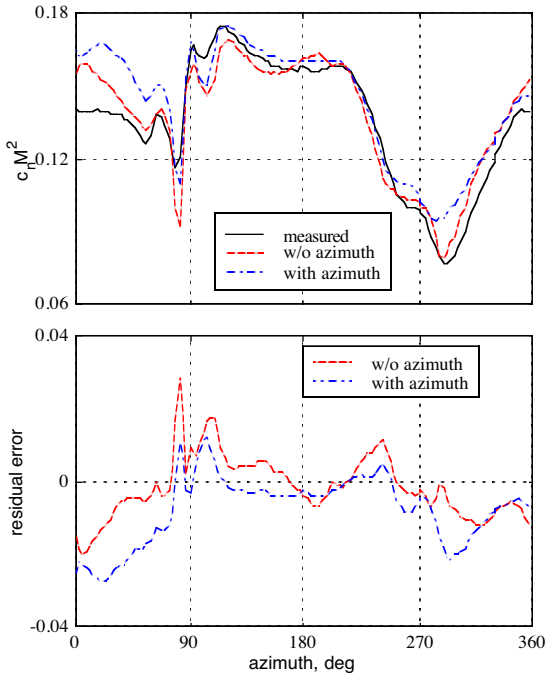


**a: subset is part of training set**

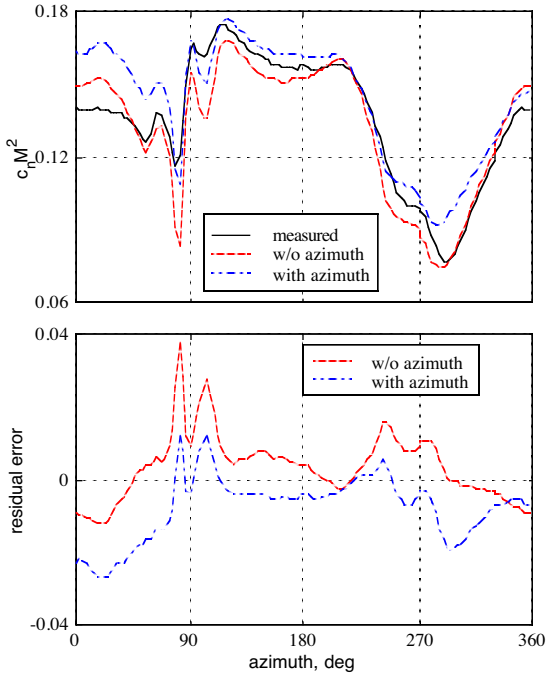


**b: subset is not part of training set**

**Fig. 31. Measured versus estimated airloads (LH3-nn-model; without and with azimuth angle as input) and residual error as function of azimuth angle for database subset #10 (0.62R, $\alpha$=+2°, $c_T/\sigma$=0.128)**

## Airloads Estimation at Intermediate Radial Locations

The evaluation of the regression and neural network models thus far has been restricted to the estimation of airloads from leading edge pressure data at the radial stations where, in general, detailed chordwise pressure data were available (r/R=0.96, 0.90, 0.82, 0.72, 0.62, 0.50, and 0.33). Such models might also be used to estimate the loading at intermediate radial locations (r/R=0.96, 0.90, 0.82, 0.72, 0.62, 0.50, and 0.33), where only 3.5% chordwise pressure data are available. is. Given that neural network models with three or more nodes in the hidden layer performed better then regression models, the discussion here is limited to a LH3-nn-model.

The LH3-neural networks, trained against the $c_nM^2$ data from radial stations r/R=0.96, 0.90, 0.82, 0.72, 0.62, 0.50, and 0.33 were used to estimate the airloads at the adjacent stations using the 3.5% chordwise station's pressure data. Whenever possible the pressure data from the upper and lower blade surfaces were input to the neural network model. Input changes were made as necessary. For instance, no lower surface pressures were available at r/R=0.50 (see Table 1). Therefore, the 0.50R-nn-model only used the upper surface pressure as input and this model was subsequently used to estimate the airloads at r/R= 0.56 and 0.42, using only the upper surface pressure from these stations, even though upper and lower $c_pM^2$ data were available at these two radial locations.

For the initial evaluation of the ability of neural network models trained for one radial station to estimate airloads at adjacent radial stations, the LH3-nn-models were used to estimate the airloads at an adjacent radial location, for which the airloads were known as well. Note that the radial distance between stations in this case is of the order of 0.1R. For the intermediate radial stations this distance would be 0.05R. NN-model inputs are $\alpha$, $C_T/\sigma$, and $c_pM^2$ at 3.5% chord at the radial location of interest. Models without and with azimuth input were evaluated. Airloads estimates for data subset #3 ($\alpha$=-2°, $c_T/\sigma$=0.089) are shown as representative of the twelve test conditions in the database.

Figure 32 shows the measured airloads at 0.90R and the estimated airloads using the nn-models, trained against the 0.96R- and 0.82R-data. The 0.82R-model's estimates show good agreement with the measured airloads. The 0.96R-model with azimuth input shows the correct trends, but the estimate is vertically offset from the measured loading.

Similar evaluations were done for 0.82R, using the 0.72R and 0.90R-nn-models (Fig. 33) and for 0.72R, using the 0.62R and 0.82R models (Fig. 34). Figure 33 shows that the 0.90R-nn-models are performing well in estimating the 0.82 airloads. The 0.72R-nn-models show the correct trends as function of azimuth, but are vertically offset from the measured airloads. Figure 34 shows that the nn-models, in general, provide the correct airloads-trends around the azimuth, but that the load traces are vertically offset.

Representative airloads estimates for intermediate radial locations 0.93R and 0.56R are shown in Figs. 35 and 36, respectively, for data subset #3. The 0.50R-nn-model in Fig. 36 utilizes only the upper surface pressure as an input, since the lower surface pressure transducer was non-operational (see Table 1). Very similar trends in airloads estimates are seen around the azimuth, but the traces are again vertically offset, especially at the 0.56R location (Fig. 36). Better agreement between the curves can be obtained by adjusting the nn-output node's bias term to represent the mean $c_nM^2$-level at the considered radial station. One option to determine this bias term is to perform a spline curve fit of the mean $c_nM^2$-values as function of radial location for those stations for which detailed pressure data are available.

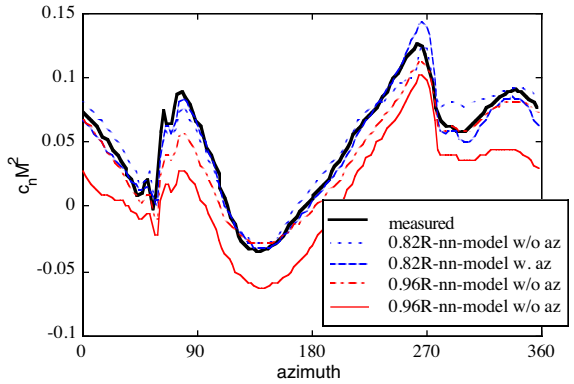


**Fig. 32. Airloads estimation at station 0.90R ($\alpha$=-2°, $c_T/\sigma$=0.089)**

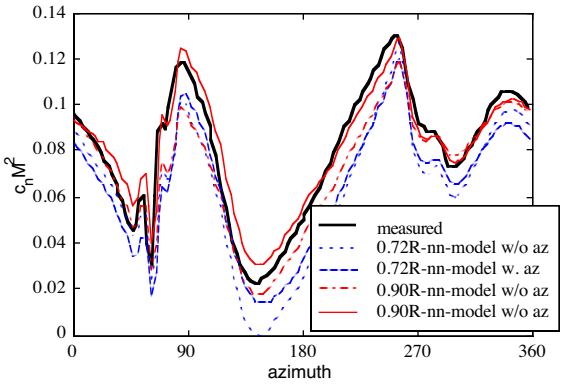


**Fig. 33. Airloads estimation at station 0.82R ($\alpha$=-2°, $c_T/\sigma$=0.089)**

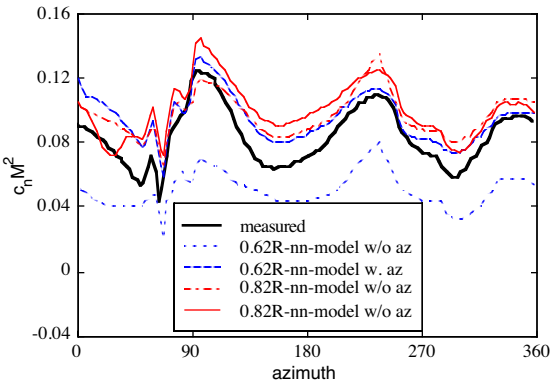


**Fig. 34. Airloads estimation at station 0.72R ($\alpha$=-2°, $c_T/\sigma$=0.089)**

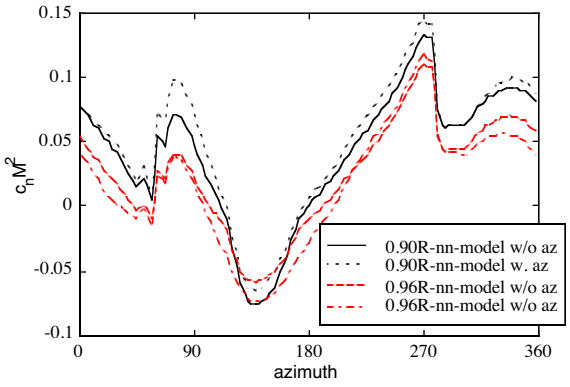


**Fig. 35. Airloads estimation at intermediate station 0.93R ($\alpha$=-2°, $c_T/\sigma$=0.089)**

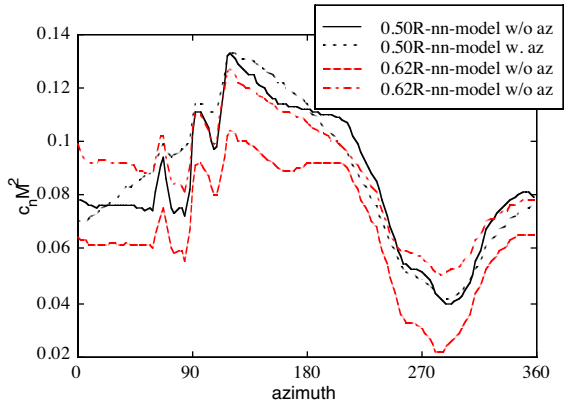


**Fig. 36. Airloads estimation at intermediate station 0.56R ($\alpha$=-2°, $c_T/\sigma$=0.089)**

## Concluding remarks

Detailed chordwise pressure data at seven radial stations were acquired for the Tilt-Rotor Aeroacoustic Model (TRAM) in the Duitse-Nederlandse Wind Tunnel (DNW). These pressure data were integrated to obtain the local blade section normal force. Pressure data at 3.5%-chord were acquired at seven additional radial stations. Linear regression models and neural network modes were evaluated in their ability to estimate the blade section airloads from leading edge pressures and representative test conditions for twelve test conditions of the TRAM pressure database. These test conditions represent forward flight at $\mu$=0.15, rotor thrust $C_T/\sigma$=0.089 and 0.128, and shaft angle of attack from –10° (forward) to -10° (aft).

The ability of regression and neural network models to fit the (training) database was evaluated first.

Neural networks with two or more nodes in the hidden layer were seen to provide better airloads estimate than linear regression models. Increasing the number of nodes in the hidden layer tends to improve the airloads estimation, but incremental improvements are small beyond three or four nodes.

Using upper surface pressure data only provides better airloads estimates than using only lower surface pressure data. At the outboard radial locations, the airloads estimation is greatly improved by using both upper and lower pressure data. At the 0.62R station the inclusion of lower pressure provided only marginal improvements over the models using only upper surface pressures.

Input of azimuth angle into the neural network model improved the estimation by correcting for $c_n$ leading $c_p$ over a major region of the azimuth. However, additional work is required to ensure that the airloads at 0° and 360° are in agreement.

Using 2.0% chordwise station data provided better airloads estimates at the outboard radial location than using 3.5% or 6.5% chord pressures. For radial stations inboard of 0.82R using the 3.5% and 6.5% chordwise pressures provided more accurate airloads estimates than using 2.0% chord pressures; this relative improvement increased for the more inboard stations.

The ability of a neural network to estimate the airloads from pressures of check-data-sets was evaluated; i.e, for data which were not part of the data against which the model was trained. The network's hidden layer contained four nodes with one linear and three tangent hyperbolic activation functions. The pressures at the 3.5% chordwise station were used as inputs as were thrust, shaft angle of attack, and azimuth angle. The neural network model performed well in estimating check-data airloads if the model was trained against data from that same radial location.

The neural network model performed reasonably well in estimating airloads at adjacent radial locations in that the airloads trend with azimuth was captured. However, the mean value of the estimate was in error, which is directly related to the bias term in the network's output layer. This term needs to be determined separately, for instance from fitting the mean airloads versus radial location curve.

## Future Work

Azimuth was used in the present investigation as a neural network input in an attempt to correct for $c_n$ leading $c_p$. Alternate methods for performing this correction will be investigated. Changes to the neural network models and inputs are also planned to improve the models capability in estimating the correct level of the airloads at the intermediate radial stations, where only pressure data at the 3.5% chordwise station are available.

Neural networks will be used to fill-out the TRAM airloads database. The training database against which selected neural network models are trained will be expanded to include points from all 98 identified test conditions, for which both leading edge pressure data and airloads are available in the TRAM database. These trained networks will subsequently be used to estimate the airloads at test conditions for which leading edge pressure data are available (same radial station) and will also be used to estimate the airloads at the intermediate radial locations, having only pressure transducers at the 3.5% chordwise station.

## References


1 Young, L.A., "Tilt Rotor Aeroacoustic Model (TRAM): A New Rotorcraft Research Facility," Heli Japan 1998: American Helicopter Society International Meeting on Advanced Rotorcraft Technology and Disaster Relief, Nagarafukumitsu, Gifu, Japan, April 1998.

2 Swanson, S.M.; McCluer, M.S.; Yamauchi, G.K.; and Swanson, A.A. "Airloads Measurements from a 1/4-Scale Tiltrotor Wind Tunnel Test," 25th European Rotorcraft Forum, Rome, Italy, September 1999.

3 Johnson, W. "Calculation of Tilt Rotor Aeroacoustic Model (TRAM DNW) Performance, Airloads, and Structural Loads," American Helicopter Society Aeromechanics Specialists' Meeting, Atlanta, Georgia, November 2002.

4 Johnson, W. "Influence of Wake Models on Calculated Tiltrotor Aerodynamics," American Helicopter Society Aerodynamics, Acoustic, and Test and Evaluation Technical Specialists' Meeting, San Francisco, CA, January 2002.

5 Riley, J., Padfield, G., and Smith, J., "Estimation of Rotor Blade Incidence and Blade Deformation from the Measurement of Pressures and Strains in Flight," Fourteenth European Rotorcraft Forum, Milano, Italy, September 1988.

6 Tarttelin, P.C., "Rotor Aeromechanics Research with the RAE Research Lynx – the Experimental Facility and Test Programme," Paper No II.7.4.1, Sixteenth European Rotorcraft Forum, Glasgow, United Kingdom, September 1990.

7 Brotherhood, P., and Riley, M.J., "Experimental Techniques in Helicopter Aerodynamic Flight Research," Paper No. 9, Agard-R-781, April 1990.

8 Spiegel, P., "BVI Noise Prediction Starting from Blade Pressures Measured at Few Points," 56th Annual Forum of the American Helicopter Society, Virginia Beach, Virginia, May 2000.

9 Nφrgaard, M., "Neural Network Based System Identification Tool Box (version 1.1; for use with Matlab®)," Tech. Report 97-E-851, Department of Automation, Technical University of Denmark, 1997.